

An Analytic Model for Cost-Benefit Analysis of Dataflows in DNN Accelerators

Hyoukjun Kwon¹, Michael Pellauer², and Tushar Krishna¹

¹Georgia Institute of Technology, Atlanta, Georgia

²NVIDIA, Westford, Massachusetts

hyoukjun@gatech.edu, mpellauer@nvidia.com, tushar@ece.gatech.edu

Abstract

Efficiently tiling and mapping high-dimensional convolutions onto limited execution and buffering resources is a challenge faced by all deep learning accelerators today. We term each unique approach as *dataflow*. The dataflow determines overall throughput (utilization of the compute units) and energy-efficiency (reads, writes, and reuse of model parameters and partial sums across the accelerator’s memory hierarchy). In this work, we provide a first-of-its kind framework called MAESTRO to formally describe and analyze CNN dataflows. MAESTRO uses a set of concise pragmas to describe three kinds of data reuse - spatial, temporal, and spatio-temporal. It predicts roofline performance and energy-efficiency of each dataflow when running neural network layers, and reports the hardware resources (size of buffers across the memory hierarchy, and network-on-chip (NoC) bandwidth) required to support this dataflow. Using MAESTRO, we demonstrate trade-offs between various dataflows, and demonstrate the potential benefits of a hardware substrate with a specialized NoC that can support adaptive dataflows.

1. Introduction

Convolutional neural networks (CNN) are one of the most popular deep learning approaches for image classification, face recognition, web search, and video processing [11, 25, 7] today, having exceeded human accuracy for many of these traditionally challenging problems. They are being increasingly deployed for real-time processing on edge devices with applications across gaming, self-driving cars, photo tagging, surveillance, and so on. Unfortunately, modern CNNs require billions of computations, placing extreme demands on performance and energy-efficiency on the hardware they run on.

Specialized accelerators (ASICs and FPGAs) have emerged for addressing this challenge [4, 3, 2, 20, 21, 10]. Many of them are spatial in nature - i.e., they are built using an array of processing elements (PEs) and use direct communication instead of via memory for energy-efficiency. These accelerators leverage the observation that CNN processing inherently relies on the same filters convolving with multiple input images, and vice-versa, providing opportunities for *data reuse*. As a simple example, VGG16’s CONV3_2 layer requires 1.85B MAC operations, but has less than 1M *unique* weights, inputs and outputs. Thus, recent accelerators have tried to keep weights or inputs or partial outputs *stationary* within on-chip processing

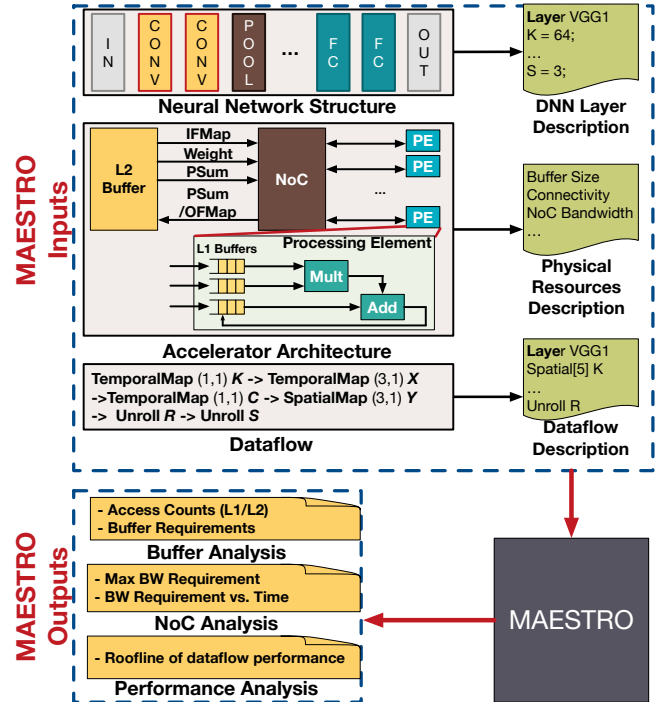


Figure 1: MAESTRO’s tool flow. elements (PEs) while streaming the other data types through the array. This is known as *dataflow*.

Coming up with the right dataflow is however an open research question today. Convolutions are deeply nested multiply-accumulate loops. There are literally millions of ways of partitioning these loops to map the billions of computations over hundreds of compute units - each of which results in a unique dataflow and corresponding data reuse. Moreover, throughput and energy efficiency of a dataflow can dramatically change depending on both the DNN topology (i.e., layer shapes and sizes), and accelerator hardware resources (buffer size, and network-on-chip (NoC) bandwidth and connectivity). The research community today lacks any formal framework to model and reason about the performance and energy-efficiency of different dataflows.

We present MAESTRO (Modeling Accelerator Efficiency via Spatio-Temporal Resource Occupancy), an analytical tool for modeling and evaluating the performance and energy-efficiency of CNN dataflows. Fig. 1 presents an overview. Our key novelty is a methodology to formally describe dataflows using five concisely defined pragmas over nested loops of convolutions. We show that the “stationary”-based taxonomy

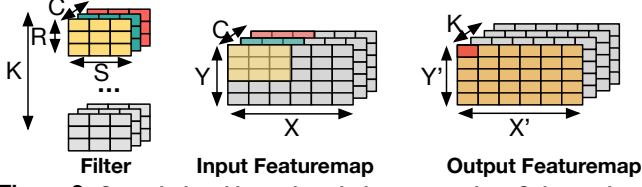


Figure 2: Convolutional layer description convention. C: input channel, R,S: filter row, column, K: output channel, Y,X: input row, column.

```

for(int ki = 0; ki < K; ki++) //Loop_K
  for(int ci = 0; ci < C; ci++) //Loop_C
    for(int yi = 0; yi < Y; yi++) //Loop_Y
      for(int xi = 0; xi < X; xi++) //Loop_X
        for(int ri = 0; ri < R; ri++) //Loop_R
          for(int si = 0; si < S; si++) //Loop_S
            O[k][x][y] += W[k][c][r][s] * I[c][y+r][x+s]

```

Code 1: 6D convolution code over one image

introduced by prior work such as Eyeriss [4] is not sufficient for the full description of the dataflow, and is captured by one of our pragmas. We provide a concise DSL that allows users to input the neural network structure (shape/size), hardware resource description (buffer size and interconnect topology/bandwidth), and desired dataflow using our pragmas. MAESTRO computes the maximum performance (roofline throughput) and hardware resources (buffer sizes and NoC bandwidth) required to achieve this performance. It also produces buffer access and link traversal counts across the memory hierarchy, which can be plugged into an energy model.

Using two case studies, we demonstrate how MAESTRO can be used at design-time, for providing quick first-order metrics at design-time when hardware resources (buffers and interconnects) are being allocated on-chip, and compile-time when different layers need to be optimally mapped for high utilization and energy-efficiency.

The rest of the paper is organized as follows. Section 2 characterizes dataflows in CNN accelerators. Section 3 presents MAESTRO. Using MAESTRO, Section 4 presents two case studies - comparing different dataflows, and demonstrating the benefits of adaptive dataflow support in hardware. Section 6 discusses related work and Section 7 concludes.

2. Dataflows in CNN Accelerators

CNNs consist of convolutional, pooling, and fully-connected layers. Among these layers, convolutional layers are significant in the amount of computations and the size of required weight/input data [24]. As presented in Fig. 2, the computation in convolutional layers is often implemented as a sliding window operation with MAC (Multiplication-Accumulation). Code 1 describes the operations as six nested for-loops.

Our discussion models the target accelerator as a spatial collection of processing elements (PEs), where each PE houses a MAC and a local “L1 buffer”, as shown in accelerator architecture in Fig. 1. The PEs are interconnected internally to each other, and to a shared “L2 buffer” by a network-on-chip (NoC), as shown in Fig. 1. This is an abstract model - a real implementation might group multiple PE’s together to create

a larger PE, the L1 could be a single latch or a FIFO or a scratchpad, the NoC could be hierarchical buses [4], systolic, tree, crossbar, and so on.

Since the multiplications in Code 1 are all independent, accelerator architectures can re-order and sub-tile the computations for efficiency and parallelism. This is necessary to limit off-chip accesses, because the size of the input feature map (upto 6.5MB in VGG16) and weight values (upto 4.5MB in VGG16) is too large to be loaded at once on to L1 buffers. These sizes also mean that strategies for sequencing the computation and splitting (tiling) data onto spatially deployed PEs is a large design space exploration problem by itself.

2.1. Definition of Dataflow

Because of the complexity of the loop nest as shown in Code 1, choosing the best dataflow for a given network layer on a given accelerator is not intuitive to describe or design.

To address this challenge, we take a *variable-centric* approach, which regards the mapping of weights/inputs as equivalent to assigning iteration variables to each PE. For example, if we assign $(ki, ci, yi, xi, ri, si) = (3, 4, 5, 6, 0-2, 0-2)$ to a PE, we observe that the PE should receive nine weights ($W[3][4][0-2][0-2]$) and one input ($I[4][5][6]$). This approach provides a better abstraction than identifying the exact weight-s/inputs to assign to each PE (data-centric approach) because it converts the 6D array mapping problem into a six-variable assignment problem.

2.2. Elements of Dataflow

Loop-ordering Changing the order of loops in Code 1 affects the data reuse patterns in each PE. For example, if we iterate in the order of $K \rightarrow C \rightarrow Y \rightarrow X \rightarrow R \rightarrow S$ and assign each X loop iteration across PEs, weight values within the same channel can remain in each PE until the channel iteration variable ci increases. However, if we iterate in an order of $K \rightarrow R \rightarrow S \rightarrow C \rightarrow X \rightarrow Y$ and assign each C loop iteration across PEs, input feature map values within the same channel can remain in each PE. We probably cannot keep weight values because the reuse time is over two inner loops (X, Y), much larger than a typical PE’s L1 buffer size. This means that the *same weight* might be read multiple times over the course of the computation from the shared L2 buffer. Thus, based on the CNN sizes, the buffer size in each PE, and the dataflow, the number of L1 (local registers) and L2 (shared buffer) read/writes of a dataflow change, as we will show later in Fig. 17.

Spatial and Temporal Mapping Spatial mapping enables individual PEs to process different sets of iteration variables at the same time. When the number of compute units or local buffer is not sufficient to cover a given spatial mapping, implicit temporal mapping is necessary—the original dataflow graph is conceptually “folded” onto a physical unit over time. For example, if the feature map width $X = 4$ and we spatially map X over two PEs, PE0 and PE1 can process $xi = 0$ and

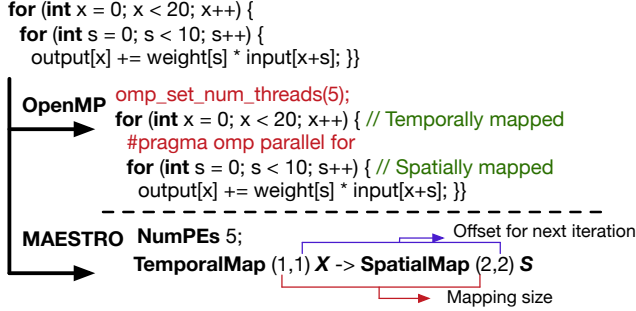


Figure 3: An 1D convolution example and OpenMP and MAESTRO description of the same mapping.

$xi = 1$, respectively, at cycle 0. And then, PE0 and PE1 process $xi = 2$ and $xi = 3$, respectively, at cycle 1.

Temporal mapping indicates that a PE can process different set of iteration variables over time, which effectively folds the compute unit requirement for full parallel execution to the time domain. For example, a PE could first process $ki = 0$ between cycles 0–9, and $ki = 1$ between cycles 10–19. Temporarily mapped variables can result in *stationary* data (inputs, weights, or partial outputs), using the taxonomy introduced in Eyeriss [4], which requires local buffer to store this stationary data over time.

Tiling The granularity of spatial and temporal mapping can be onto separate PEs, or coarse-grained groups of PEs, which we call a tile. For example, Flexflow [16] organizes PE into multiple rows and assigns operation for one output pixel to one of the PE rows. In this case, variables K , X , and Y are temporally mapped on a PE row but variables C , R , and S are spatially mapped to PEs in the PE row. The tile can be organized into higher dimensions than two.

2.3. Describing Dataflows

Based on the elements discussed in Section 2.2, we propose a method to formally describe dataflows using a combination of five pragmas that includes all the elements of dataflow, loop ordering, spatial/temporal mapping and tiling, as presented in Fig. 5. The pragmas follows the philosophy of pragma-based parallel programming libraries, such as OpenMP [5], which provides a concise way to describe loop parallelization as an 1D convolution mapping example in Fig. 3 shows. We use the example in Fig. 3 as a representative example in this paper. Fig. 7 (a) describes the resulting variable mapping from the MAESTRO pragmas in the example in Fig. 3 showing the capability to describe both of the temporal and spatial mapping. In addition to temporal and spatial map pragmas, MAESTRO provides loop unroll and PE tiling pragmas, which enables the description of various dataflows. We highlight the syntax and semantics of the pragmas in Section 3.

2.4. Data Reuse

Maximizing data reuse is the prime target of many accelerators as it improves both the throughput and energy efficiency. Data reuse reduces the number of energy-consuming L2 reads and

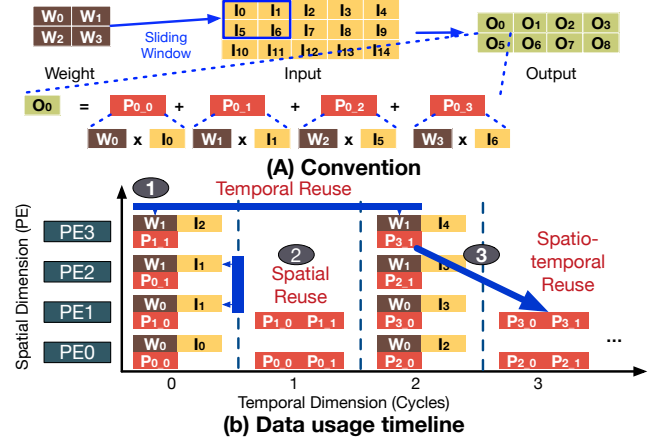


Figure 4: Timeline of a row-stationary (logical PE version) [4] accelerator with four PEs. We show example data reuse opportunity for three data reuse classes we introduce.

writes (which translates to fewer DRAM reads and writes), in turn translating to reduced bandwidth requirements from the L2 and the NoC implementations within the accelerator. We define three classes of data reuse.

Temporal data reuse (Stationary data): Temporal data reuse opportunity highlighted by the stationary taxonomy in Eyeriss [4] is based on non-shared variables among data classes. For example, if the innermost spatially-mapped loop variable is K , although the target weight pixel changes every K loop iteration, the target input pixel does not because inputs do not have a K dimension. The stationary data class is determined by the loop order and *innermost spatially mapped loop*. For example, weights in a row-stationary dataflow [4] are reused in temporal dimension as illustrated in Fig. 4, in which weight is stationary in K and C dimension. In this example, Each PE has one R and one S value until an entire row is processed; thus weight is fully-stationary for each Loop Y iteration. To exploit temporal reuse, an accelerator needs a local L1 buffer in each PE with sufficient size to stage data until their next reuse.

Spatial data reuse (Multicast data): Spatial data reuse opportunity is based on temporal mapping and sliding window halo. For example, in Fig. 4 (b), because of the halo from SPATIAL_MAP (2, 1), I_1 is shared between PE1 and PE2 at the same time. Rather than reading the data twice from the L2 buffer, an accelerator can read only once and multicast I_1 to PE1 and PE2. To exploit spatial reuse across PEs, an accelerator needs a NoC that supports multicasting (bus, tree, etc.). At a finer granularity, spatial reuse can be exploited even from the L1 (e.g., fanning out an input to multiple weight datapaths via internal wires).

Spatio-temporal data reuse (Local-forwarded data): Also called producer/consumer parallelism, this is based on sliding window halo over implicit temporal mapping. For example, in Fig. 4, the second partial sum for the third output, denoted as $P3_1$, is forwarded from PE3 to PE1 to be used in the different time. To exploit spatio-temporal reuse, an

```

Constants Definition
LayerName ∈ (String) sz, ofs, bw ∈ (Integer)
LoopVar := K | C | R | S | Y | X
Layer := CONV | POOL | FC

Physical Resource Description
PEInfo := NumPEs (sz)
BufferInfo := L1Size (sz) | L2Size (sz)
NoCInfo := Bandwidth (bw)

DNN Layer Description
LoopSz := (LoopVar) (sz)
LayerInfo := Layer (LayerName) (LoopSz)* endLayer

Dataflow Description
PragmaBody := Tile (sz) | Spatial_Map (sz,ofs)
| Temporal_Map (sz,ofs) | Unroll
Pragma := (PragmaBody) (LoopVar)
Dataflow := (Pragma)*
HWInfo := (BufferInfo)* (NoCInfo)* (PEInfo)
MAESTRO := (HWInfo) (LayerInfo) (Dataflow)

```

(a) Syntax

(b) Example

Figure 5: The syntax of MAESTRO DSL and an example of it. (a) The unit of size is the number of elements (e.g., L1size 256 indicates the size of 256 elements, 512 Byte with 16-bit fixed point data). We use * as a shorthand for semicolon-terminated repetition. (b) The example is for the WS dataflow from Table 1

accelerator needs local forwarding links among PEs, which could be dedicated links to neighbors. General topologies such as meshes can also support spatio-temporal reuse using the standard arbitrated links.

Given the description of an architecture and buffer hierarchy, MAESTRO assumes that the accelerator exploits all three data reuse opportunities to evaluate the potential of the dataflow.

3. MAESTRO: Dataflow Analysis Framework

3.1. MAESTRO Domain-specific Language

3.1.1. Hardware and DNN layer description Fig. 5 presents the syntax of MAESTRO DSL and an example hardware, layer, and dataflow description using it. For the layer description, users can specify the shape and size of each dimension of a convolutional layer. For the hardware description, users can specify L1 (i.e., private/local) and L2 (i.e., shared/global) buffer (i.e., FIFO/scratchpad) sizes, and the NoC average hops, bisection bandwidth, and ingress/egress bandwidth from/to L2. For the dataflow description, users can specify various mapping and tilings using the pragmas presented in Section 2.3. Fig. 5 (b) shows an example.

3.1.2. Dataflow pragmas Dataflow description syntax includes dataflow pragmas we introduced in Section 2.3 allows users to describe a variety of dataflows. MAESTRO DSL includes four pragmas, temporal and spatial map, unroll, and tile, whose syntax is as described in Fig. 5. We highlight the semantics of each dataflow pragma.

Temporal and spatial map. Temporal and spatial mappings are fundamental pragmas to describe dataflow. Temporal map is a variable mapping pragma that applies the same variable sets to the tiles (PEs in base case; when no tile pragma is used). On the other hand, spatial map enables to map different variable sets to each tile simultaneously allowing users to exploit parallelism. Temporal and spatial map has two arguments, size and offset. The size argument represents the number of mapped

Pragmas Attribute	TemporalMap (Sz, OfS) Var	SpatialMap (Sz, OfS) Var	Unroll	Tile (Sz)
Map size	Sz	Sz	LoopSz(Var)	-
Temporal offset	Ofs	LoopSz(Var) / OfS / tiles[Var].Sz	0	-
Spatial offset	0	Ofs	0	-
Tile index mapping	-	-	-	tiles[var][idx] = tiles[var][idx*Sz : idx*(Sz+1)-1]

(a) Mapping attributes of each loop set by dataflow pragmas

```

Input: loop list (lp_lst)
Output: tile list with variable mapped (tiles)
Procedure IterateMapping
  finished = true;
  for each loop in lp_lst from innermost loop
    if(finished) then
      finished &= (last_tile.base + last_tile.map_sz > loop.bound);
      for each tile in tiles[loop.var]
        tile.base = tile.base + tile.tp_ofs + tile.sp_ofs * tile.idx;
        tile.map(tile.map_sz);
      end
    end
  end
endProcedure

```

* tile.map(size): map variables in the range of [tile.base, tile.base + tile.map_sz)
* Pervasive mapping: tile.map performs mapping for every sub tiles in tiles[var][tile_idx]

(b) Mapping model based on attributes

Figure 6: Mapping semantics of MAESTRO dataflow pragmas. MAESTRO scans dataflow pragmas from the innermost loop and constructs tiles by updating index mapping structures at each loop. After the tile construction, it scans pragmas from the outermost loop to assign three attributes described in (a). (b) shows how MAESTRO determines variable mapping in each iteration of each loop.

variables and the offset argument defines how the mapped variables are updated when the PE array finishes a spatial or temporal iteration. Fig. 6 describes precise semantics how temporal and spatial map determines mapped variables at each iteration. The temporal offset of spatial map shows how implicit temporal folding happens with spatial maps. When the number of tiles is not sufficient to cover entire variables in the spatially mapped loop, then the tile array moves onto the next set of spatial mappings. This process is repeated until the spatial map covers entire variables in the corresponding loop. Fig. 7 (a) shows how the argument affects the map size and the update of mapped variable over space (PEs) and time.

Unroll. Unroll pragma performs loop unrolling. Unroll embeds all the operations within an unrolled loop to its next upper loop, which results in the mapping of entire unrolled loop variable values. Therefore, it does not involve any temporal or spatial foldings and yields the same effect as TEMPORAL_MAP (loop_size, loop_size) of the unrolled loop variable. Fig. 7 (b) presents an example of UNROLL. As discussed, the example maps all the s values in [0, 10) to each PE.

Tile. Tile is the fundamental mapping target of variables. In the base case, when no tile pragma was placed, each tile is a PE. Tile pragma groups the PEs or tiles up in the size of tile pragma. For example, in Fig. 7 (c), TILE (5) X groups five tiles (in this base case, PEs) to construct a new tile. Mapping of X and its upper loops target the tiles, and mapping of variables in inner loops target the PEs (subtiles in case of multiple tile pragmas). Multiple tile pragmas constructs hierarchical tiles by performing grouping of tiles present at the loop level. Tile pragmas are processed from the innermost loop to outermost

Accelerator	Dataflow Strategy	Dataflow
Example for this work	No Local Reuse (NLR)	TEMPORAL_MAP (1,1) K → TEMPORAL_MAP (1,1) C → TEMPORAL_MAP (1,1) Y → TEMPORAL_MAP (1,1) R → TEMPORAL_MAP (1,1) S → SPATIAL_MAP (1,1) X
Example for this work	Weight Stationary (WS)	TEMPORAL_MAP (1,1) K → TEMPORAL_MAP (1,1) C → TEMPORAL_MAP (3,3) Y → SPATIAL_MAP (3,1) X → UNROLL R → UNROLL S
ShiDiannao [6]	Output Stationary (OS)	TEMPORAL_MAP (1,1) K → TEMPORAL_MAP (1,1) C → TEMPORAL_MAP (3,1) Y → SPATIAL_MAP (3,1) X → UNROLL R → UNROLL S
Eyeriss [4]	Row-stationary	TEMPORAL_MAP (1,1) K → TEMPORAL_MAP (1,1) C → SPATIAL_MAP (3,1) Y → TILE (Sz(R)) X → TEMPORAL_MAP (3,1) X → SPATIAL_MAP (1,1) R → UNROLL S
NVDLA [2]	Weight Stationary	TEMPORAL_MAP (1,1) R → TEMPORAL_MAP (1,1) S → TEMPORAL_MAP (64,64) C → TEMPORAL_MAP (1,1) Y → TEMPORAL_MAP (1,1) X → SPATIAL_MAP (1,1) K

Table 1: A list of dataflows with description based on pragmas introduced in Section 3.1.2 and corresponding accelerators.

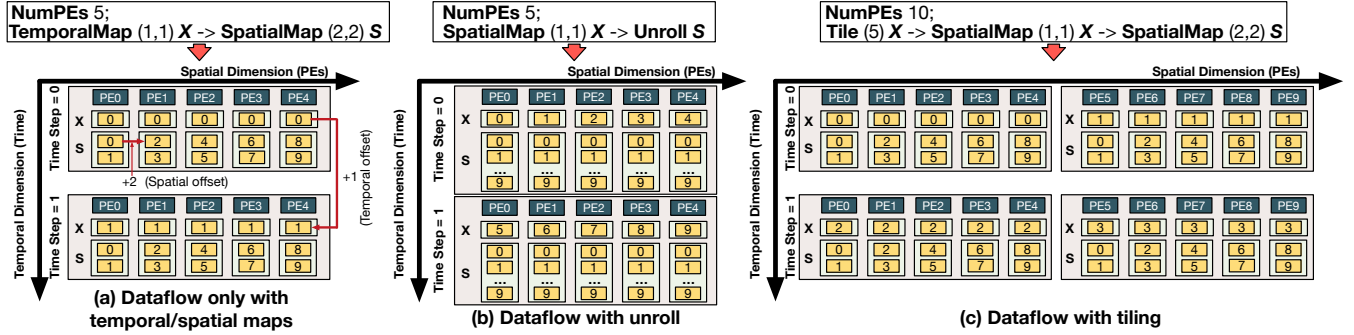


Figure 7: Examples of dataflows described with MAESTRO dataflow pragmas for the 1D convolution described in Fig. 3 and corresponding variable mapping schedules. We show spatial and temporal offsets only in (a). The numbers in boxes under each PE array correspond to variable values mapped at the time step specified in the left side of each PE array box. Note that boxes are for each variable (x and s, in this example).

Variable	Output Channel (K)	Input Channel (C)	Filter Height (R)	Filter Width (S)	Input Height (Y)	Input Width (X)
Data class						
Output Activation	O	X	O	O	O	O
Input Activation	X	O	X	X	O	O
Filter Weights	O	O	O	O	X	X

* Output height = Y-R+1, Output width = X-S+1

Figure 8: Correlation among variables & data classes in 6D conv.

loop to support correct hierarchical tile structure.

As we observed in this subsection, dataflow pragmas include all the elements of dataflows discussed in Section 2.2. The dataflow pragmas allows to change loop order by re-ordering pragmas, enables spatial and temporal mapping by dedicated pragmas, and supports constructive tiling with TILE pragma. Now we discuss how MAESTRO analyze the dataflow written in dataflow pragmas and generates statistics about cost and benefit of the input dataflow.

3.2. MAESTRO Analysis Engine

The key concept for precise buffer access counts and runtime modeling is data reuse discussed in Section 2.4. If the accelerator does not utilize any spatial or temporal reuse, the analysis is trivial. However, understanding data reuses and applying that to cost estimation is a complex problem. MAESTRO analyzes temporal and spatial reuse by identifying the total number of mapped variables and the number of uniquely mapped variables for each spatial iteration. For simplicity, we restrict the number of spatially mapped loops as one. Multiple spatially mapped loops can be analyzed by recursively applying the method we discuss.

3.2.1. Spatially and temporally mapped volume analysis

To compute the number of data points per tile at spatial mapped loop mapped by variable mappings, which we refer as mapped volume, MAESTRO simply multiply the number of mapped

<p>Input: dataflow description in MAESTRO pragmas (<i>df_desc</i>)</p> <p>Output: The total or uniquely mapped size of a data class on a PE (<i>mp_sz</i>)</p> <p>Procedure AnalyzeVariableMapping:</p> <pre> for each pragma in df_desc switch(pragma.class) case TemporalMap: M[pragma.var] = pragma.map_sz; SU[pragma.var] = 0; TU[pragma.var] = (pragma.map_sz > pragma ofs)? pragma ofs : pragma.map_sz; case SpatialMap: M[pragma.var] = pragma.map_sz; SU[pragma.var] = (pragma.map_sz > pragma ofs)? pragma ofs : pragma.map_sz; TU[pragma.var] = pragma.map_sz; case Unroll: M[pragma.var] = pragma.loop_sz; SU[pragma.var] = 0; TU[pragma.var] = pragma.loop_sz; end end endprocedure </pre> <p>* M: Mapped variables * SU: Spatially unique variables * TU: Temporally unique variables</p>	<p>(a) Temporally/spatially unique and non-unique number of variables analysis</p> <pre> //MV: Mapped volume MV[Weights] = M(K) x M(C) x M(R) x M(S) MV[Inputs] = M(C) x M(Y) x M(X) MV[Outputs] = M(K) x M(Y) x M(X) //MSUV: Mapped spatially unique volume MSUV[Weights] = GetSpUSz(K) x GetSpUSz(C) x GetSpUSz(R) x GetSpUSz(S) MSUV[Inputs] = GetSpUSz(C) x GetSpUSz(Y) x GetSpUSz(X) MSUV[Outputs] = GetSpUSz(K) x GetSpUSz(Y) x GetSpUSz(X) //MTUV: Mapped temporally unique volume MTUV[Weights] = TU(K) x TU(C) x TU(R) x TU(S) MTUV[Inputs] = TU(C) x TU(Y) x TU(X) MTUV[Outputs] = TU(K) x TU(C) x TU(Y) x TU(X) //MSTUV: Mapped spatially and temporally unique volume MSTUV[Weights] = GetStpUSz(K) x GetStpUSz(C) x GetStpUSz(R) x GetStpUSz(S) MSTUV[Inputs] = GetStpUSz(C) x GetStpUSz(Y) x GetStpUSz(X) MSTUV[Outputs] = GetStpUSz(K) x GetStpUSz(C) x GetStpUSz(Y) x GetStpUSz(X) </pre> <p>* GetSpUSz(V) = (V. pragma.class == TemporalMap)? M(V) : SU(V); * GetStpUSz(V) = (V. pragma.class == SpatialMap)? SU(V) : TU(V);</p>
---	---

(b) Temporally/spatially unique and non-unique volume analysis for 6D convolution

Figure 9: Mapped volume analysis model in MAESTRO.

corresponding variables. This volume does not consider any reuse but represent the number of ultimately accessed data points in each spatial iteration. MAESTRO identifies the number of spatially, temporally, and spatio-temporally unique data points by analyzing the map size of each variable and offset of spatial/temporal map pragma, the bound of loops in

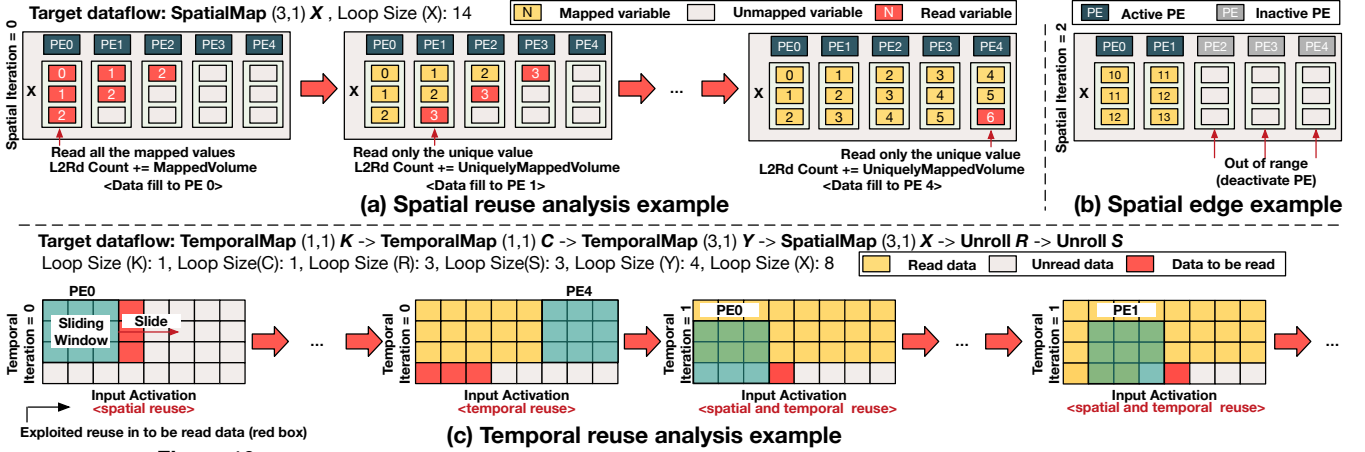


Figure 10: Simplified examples of (a) spatial reuse analysis, (b) spatial edge, and (c) temporal reuse analysis

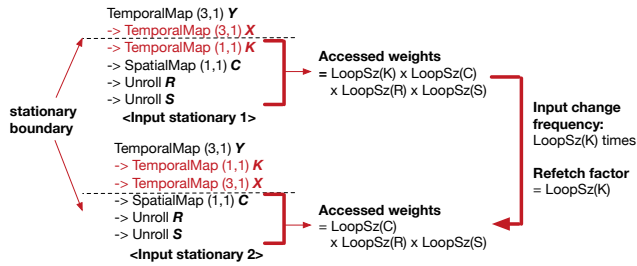


Figure 11: The difference in the lifetime of stationary data in two input stationary dataflow.

outer loops, and the correlation of each variable with a data class presented in Fig. 8. Fig. 9 presents the mapped volume analysis model of MAESTRO. MAESTRO first processes each pragma and extract the number of total, spatially unique, and temporally unique mapped variables as shown in Fig. 9 (a). Based on the mapped variable analysis, MAESTRO identifies the number of total data points (mapped volume, MV), the number of spatially unique data points (spatially unique volume, MSUV), the number of temporally unique data points (temporally unique volume, MTUV), and the number of spatially and temporally data points (spatially and temporally unique volume, MSTUV), as presented in Fig. 9 (b). The difference between mapped volume and unique volume represents the reused volume. Each unique volume represents net amount of data needs to be processed in each spatial or temporal iteration.

3.2.2. Spatial and temporal data reuse pattern analysis As recent CNN accelerator works presented [4, 9], buffer access consumes the majority of energy. Therefore, modeling buffer size to support all of the potential data reuse implied by a dataflow and buffer access counts is crucial to estimate the energy consumption of a dataflow with a given hardware configuration on an input layer. Those buffer costs depend on multiple factors including mapping size, spatial and temporal data reuse, multicasting capability, the number of active tiles at the edge of layers dimensions, the frequency of data update from upper temporal loops and so on. They are not only many but also intertwined in a complicated manner. In particular,

buffer analysis requires deep understanding of spatial, temporal, and combination of those reuse because reuse in L1 buffer reduces the number of buffer accesses to the L2 buffer. Also, we need to skip inactive PEs at the edge of spatial iterations deactivated due to variable index out of range. MAESTRO considers all of the aspects, and we described them in the detailed model description in Fig. 12 and Fig. 13. In addition to the details, we illustrates core aspects in intuitive examples in Fig. 10.

Spatial reuse. Fig. 10 (a) shows an example of spatial reuse pattern with a simplified dataflow. For simplicity, we omit all the loop variables except X. To provide the mapped variable to the first PE, because no other data points are read in the PE array, PE0 needs to read all the mapped data from L2. However, from the second PE (PE1), we can observe that only unique data is read. This implies that we need to treat the first PE as an exception in our cost model. The data read pattern relies on the spatial offset. However, in Fig. 13, we present the case of offset is one for simplicity, and because spatial offset is likely 1 because most of recent CNNs use the stride of 1 in sliding windows. Fig. 10 (b) presents another exceptional case of spatial iteration, which is edge case of spatially mapped dimension (X). In such a case, some of PEs are inactive because mapped variables to those PEs are out of range. The cost model need to precisely compute the number of inactive PEs to prevent overestimate buffer accesses. Because the exceptional cases in spatial iterations can be the common case based on the dimension of layers and number of PEs, which amplify the error in a large scale if not correctly handled, precisely modeling such cases are critical to the correctness of the model.

Temporal reuse. Fig. 10 (c) presents data reuse pattern when we consider temporal reuses. In the first temporal iteration, PEs cannot exploit temporal reuse because no temporally mapped data is read yet. However, as the second case in Fig. 10 (c) shows, when the PE array moves on to the next temporal iteration, PEs started see temporally staged data that can be reused, which results in only three unique data to read.

The reuse pattern changes immediately after the first PE in the second temporal iteration, as shown in the third case of Fig. 10 (c). In that case, because both of spatial and temporal reuse can be exploited, a PE reads only one data in the example. The unique data volume in each case depends on map sizes and offsets, unrolled loops, and the number of PEs. Spatial volume analysis (SV_(F/S)TP_(S/L)SP values) in Fig. 13 precisely model all the aspects discussed in examples in Fig. 10. In addition to aspects discussed in Fig. 10, we also need to correctly infer the lifetime of stationary data.

Lifetime of temporally reused (stationary) data. As presented in Fig. 8, because each data class has different set of correlated variables, the data volume mapped on each PE does not necessarily change at every spatial or temporal iteration. This implies the stationary data class introduced in Eyeriss [4]. However, even within the same data class stationary, the duration of keeping data stationary changes depending on details of a dataflow (map size, loop order, and so on), and this is not well studied in previous literatures. Fig. 11 shows an example how the lifetime of stationary data differs based on dataflow. In the example, the only difference of the two dataflows is the order of pragmas for variable X and K. However, this difference results in $LoopSz(K)$ times difference in the accessed weight volumes before the loop iteration breaks stationary boundary, which implies that stationary data in *input stationary 2* needs to be updated $LoopSz(K)$ times as frequent as that of *input stationary 1*. This rate also implies the refetch factor of inputs that eventually increments the number of L2 buffer access by $LoopSz(K)$ times. However, the increased cost based on short life time of stationary data, or the update frequency of stationary data, need to be considered with changes in costs of other data classes. Therefore, we still need to analyze the cost of whole data classes to classify a dataflow as efficient or inefficient. MAESTRO models the lifetime of stationary data as the update frequency, as illustrated in Fig. 12 (c), and it is used in buffer cost analysis and runtime estimation illustrated in Fig. 13 and Fig. 14. Based on the core concepts we introduced so far, we describe the buffer cost and runtime (latency) model of MAESTRO.

3.2.3. Buffer Analysis

Buffer size requirement MAESTRO defines the size of required L1 buffer as the sum of mapped volumes for each data class. This size is required to exploit data reuse opportunities implied by each dataflow descriptions. If the L1 buffer size is not sufficient, MAESTRO outputs an error that the hardware cannot support the input dataflow correctly. When user enables double buffering, the L1 buffer requirement doubles. At the cost of buffer size, double buffering is beneficial in runtime when the total delay is dominated by communication delay. The runtime analysis module also models double buffering and provides meaningful information around it.

MAESTRO defines the required size of L2 buffer as the sum of uniquely mapped volumes over one spatial iteration to support the dataflow without threshed by DRAM accesses. Un-

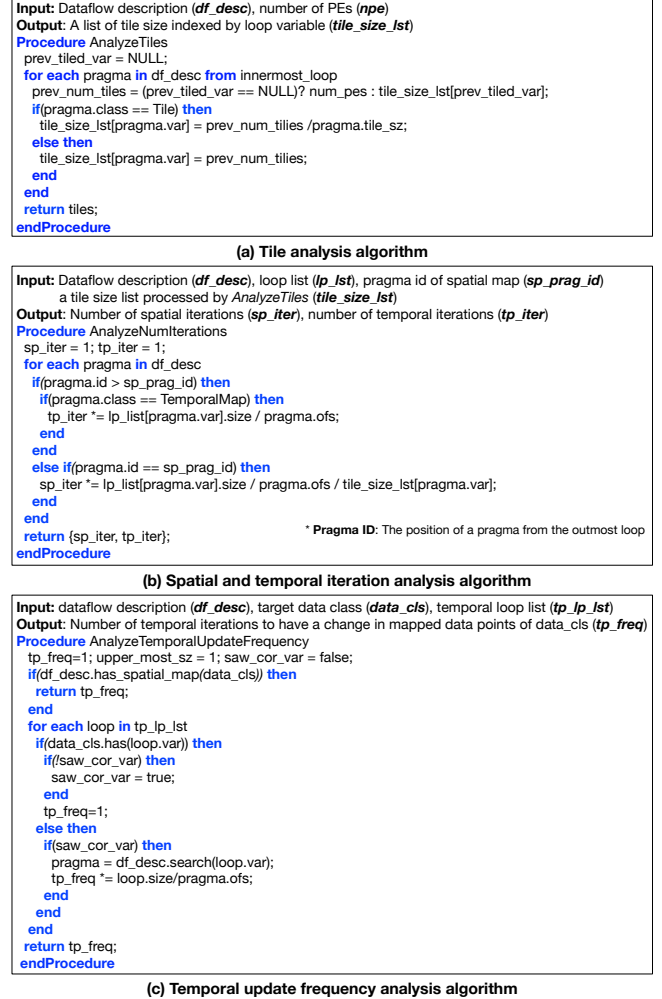


Figure 12: Tile, number of temporal/spatial iterations, and temporal update frequency analysis algorithms. Peripheral analysis modules utilizes the values computed through algorithms in (a), (b), and (c).

like L1 buffers, MAESTRO always applies double buffering to the L2 buffer because of significant DRAM access delay.

Buffer access counts Because buffer accesses on smaller buffer than the minimum size to support all the reuse rely on dynamic aspects such as buffer entry replacement policy, communication schedule and so on, MAESTRO analyze the minimum buffer access counts with the given input dataflow on input layer, which implies the energy save potential of dataflows.

Modeling L2 buffer write and L1 buffer read is relatively simple. For L2 buffer write, because we estimate the minimum number of buffer accesses, we apply the algorithmic minimum number of buffer write; the number of data points of each data class - weight, input, and output. For L1 buffer read, because local reads are not affected by any data reuse, we can easily multiply the mapped volume, number of temporal/spatial iterations, number of spatial tiles (PEs in base case without tile pragmas). However, we still need to consider the number of active tiles in the edge; when the number of tiles does not

```

//Buffer Requirements
L1BufferRequirement = 2 x (MV[Weights] + MV[Inputs] + MV[Outputs])
L2BufferRequirement = 2 x { (M[Weights] + (NumSplitter-1) x MSUV[Weights])
    + (M[Inputs] + (NumSplitter-1) x MSUV[Inputs]) }

//Data volumes required for each spatial iteration in four cases (spatial volume)
// (first/steady) temporal iteration x (steady/last) spatial iteration
// -> {first/steady, first/last, steady/steady, steady/last}
SV_FTP_SSP[in_data_cls] = tilesz_list[sp_var] * {MV[in_data_cls] + (num_sp_tiles-1)
    * MSUV[in_data_cls]}
SV_FTP_LSP[in_data_cls] = tilesz_list[sp_var] * {MV[in_data_cls] + (num_sp_edge_tiles-1)
    * MSUV[in_data_cls]}
SV_STP_SSP[in_data_cls] = tilesz_list[sp_var] * {MTUV[in_data_cls] + (num_sp_tiles-1)
    * MTSUV[in_data_cls]}
SV_STP_LSP[in_data_cls] = tilesz_list[sp_var] * {MTUV[in_data_cls] + (num_sp_edge_tiles-1)
    * MTSUV[in_data_cls]}

//Multicasting factor
Multicast_factor[in_data_cls] = MV[in_data_cls] / MSUV[in_data_cls]

//Buffer access counts
L2Wr[in_data_cls] = // Product of Loop sizes of each corresponding variable to in_data_cls
    = (NoC.multicast_support)?
    (sp_iter-1) * SV_FTP_SSP[in_data_cls] + SV_FTP_LSP[in_data_cls]
    + (tp_iter-1) * {SV_STP_SSP[in_data_cls]
    + SV_STP_LSP[in_data_cls]} / tp_freq[in_data_cls]
    : (sp_iter-1) * num_sp_tiles * MV[in_data_cls]
    + num_sp_edge_tiles * MV[in_data_cls]
    + (tp_iter-1) * { (sp_iter-1) * num_sp_tiles * MTUV[in_data_cls]
    + num_sp_edge_tiles * MTUV[in_data_cls]} / tp_freq[in_data_cls]

L1Wr[in_data_cls] = (NoC.multicast_support)? L2Rd[in_data_cls] * multicast_factor
    : L2Rd[in_data_cls];
L1Rd[in_data_cls] = tp_iter * { (sp_iter-1) * num_sp_tiles * MV[in_data_cls]
    + num_sp_edge_tiles * MV[in_data_cls]}

```

Figure 13: Buffer size requirement and access count analysis model.

divide spatially mapped dimension evenly, we have inactive PEs in the last spatial iteration.

L2 read and L1 write counts are closely related because they are sender and receiver of data. The model of L2 read counts is one of the most complicated part of MAESTRO model. In addition to exceptional cases we illustrated in Fig. 10, we also need to the multicast capability of network on chip that enables spatial data reuse and the update frequency of temporally mapped variables. All of those aspects including those introduced in Section 3.2.2 are encapsulated in the model we present in Fig. 13.

The difference between counts for L2 read and L1 write is if counting multicast as one (L2's perspective) or number of destinations (L1's perspective). Therefore L1 write counts is L2 read multiplied by corresponding multicast factor if network on chip supports multicasting. When the NoC does not support multicasting, L1 write number matches L2 read counts because the model of L2 read counts already considered individual data delivery of data can be multicasted (when supported).

3.2.4. Performance (runtime) analysis Runtime analysis requires full consideration of not only the aspects we highlighted in Section 3.2.1 but also hardware execution specific-details such as pipelining, double buffering, communication delay, and so on. The runtime analysis model of MAESTRO presented in Fig. 14 models all of those aspects. The runtime model in default applies double buffering, which prefetches data volume for the next spatial iteration and enables latency hiding of communication latency. This technique prevents long critical path (data fetch delay + compute delay + data commit delay) by overlapping data fetch delay, which results in the total delay of (max(data fetch delay, compute delay + data commit delay)). Also, MAESTRO let the number of ALUs within a PE as a parameter, which helps modeling

```

//Compute delay per spatial iteration in each PE
NumOps = M(K) x M(C) x (M(Y) - M(R) + 1) x (M(X) - M(S) + 1) // when M(Y) > M(R) and M(X) > M(S)
ComputeDelay = NumOps/NumALUs + DelayPerOps - 1 // pipelined ALUE delay

//NoC delay
NoCDelay(num_sends) = num_sends/bandwidth + avg_latency - 1 // pipelined NoC delay

```

(a) Unit compute and NoC delay

```

Input: The number of ALUs in each PE (num_alus), temporal update frequency (tp_freq),
    number of spatial iterations (sp_iter), number of temporal iterations (tp_iter)
Output: Total runtime for a given input layer (runtime)
Procedure ComputeRuntime
    runtime = 0;
    //First temporal iteration
    if(sp_iter > 1) then
        init_noc_delay = NoCDelay(SV_FTP_SSP[input]) + NoCDelay(SV_FTP_SSP[weight])
    else then
        init_noc_delay = NoCDelay(SV_FTP_LSP[input]) + NoCDelay(SV_FTP_LSP[weight])
    end
    runtime += init_noc_delay;

    if(sp_iter > 2) then //already loaded the first data sets
        L2ToL1_noc_delay = NoCDelay(SV_FTP_SSP[weight]) + SV_FTP_SSP[input]
        L1ToL2_noc_delay = NoCDelay(SV_FTP_SSP[output])
        runtime += (sp_iter-2) * max(L2ToL1_noc_delay, L1ToL2_noc_delay + ComputeDelay)
    else then
        L2ToL1_noc_delay = NoCDelay(SV_FTP_LSP[weight]) + SV_FTP_LSP[input]
        L1ToL2_noc_delay = NoCDelay(SV_FTP_LSP[output])
        runtime += (sp_iter-1) * max(L2ToL1_noc_delay, L1ToL2_noc_delay + ComputeDelay)
    end

    //Rest of temporal iterations
    if(sp_iter > 1) then
        L2ToL1_noc_delay = NoCDelay(SV_STP_SSP[weight]/tp_freq[weight]
            + SV_STP_SSP[input]/tp_freq[input])
        L1ToL2_noc_delay = NoCDelay(SV_STP_SSP[output]/tp_freq[output])
        runtime += (tp_iter-1) * (sp_iter-1) * max(L2ToL1_noc_delay, L1ToL2_noc_delay + ComputeDelay)
    else then
        L2ToL1_noc_delay = NoCDelay(SV_STP_LSP[weight]/tp_freq[weight]
            + SV_STP_LSP[input]/tp_freq[input])
        L1ToL2_noc_delay = NoCDelay(SV_STP_LSP[output]/tp_freq[output])
        runtime += (tp_iter-1) * max(L2ToL1_noc_delay, L1ToL2_noc_delay + ComputeDelay)
    end
    return runtime;
endprocedure

```

(b) Runtime estimation model

Figure 14: MAESTRO runtime analytic model. Total spatially mapped volume (SVs) in four different cases are defined in Fig. 13

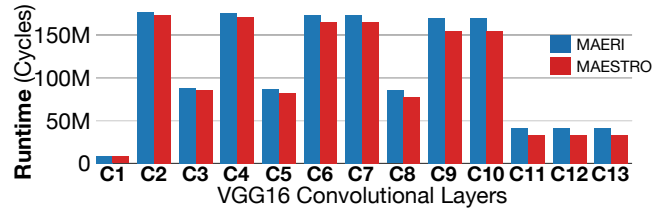


Figure 15: Runtime model validation against MAERI [15] on all of the VGG16 convolutional layers with 64 PEs. We utilize MAERI's open-source code base and hardware RTL-based cycle accurate simulation environment [1]. We model the example dataflow implemented in the testbench infrastructure using MAESTRO.

accelerators with fine-grained PEs such as SCNN [20].

3.2.5. Supported dataflows by analytic model Although MAESTRO can model a large collection of dataflows, it currently does not support arbitrary tiling that splits a loop into smaller ones and places them in arbitrary positions. MAESTRO DSL still can describe such a dataflow as multiple map pragmas placed across different tile borders with an additional syntax that specifies the split loop sizes. Also, MAESTRO currently supports only convolutions, but MAESTRO receives the data class names and correlated variable list and the implementation is designed to support arbitrary correlation of data class and variables. Therefore, with some changes in APIs, MAESTRO can support other problems such as fully connected layer or LSTMs.

Technology Node	TSMC 28nm
Implementation	RTL written in Bluespec System Verilog [19]
Number of PEs	64
Clock Frequency	200MHz
Energy Estimation	Based on Cacti [18] simulation and activity numbers from simulation
Dataflows	NLR (no-local-reuse, N), WS (weight-stationary, W), Shi (shi-diannao, S) [6], DLA [2] (D), and RS (row-stationary; Eyeriss [4], R)
Neural Network Layers	VGG16 [24] conv1 and 11 (VC1 and VC11), and PWC-net [23] conv1 (PWC1), 4 (PWC4), and 6 (PWC6).
Network-on-Chip	Crossbar switch from OpenSMART [13] (CB), Microswitch NoC [14] (MS), a two-level hierarchical bus with eight sub-clusters following SCNN and Eyeriss style [20, 4] (HB), mesh NoC [13] (MH), and FLICR (FR, this work)

Table 2: Evaluation environment description

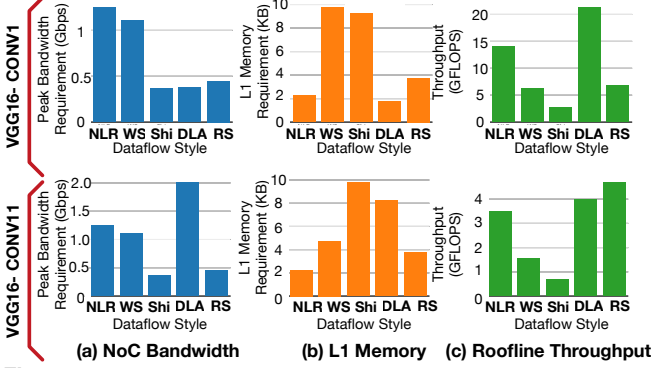


Figure 16: Tradeoff of dataflows presented in Table 1 with 64 PEs under steady iteration state (not at edge of any direction) over VGG16’s convolutional layer 1 and 11. X-axis lists up dataflow styles we evaluate. The first two Y-axis plots bandwidth (Gbps) and L1 memory (KB) requirement for entire accelerator, which are the minimum numbers to support dataflow without bottleneck from NoC and buffer. The last Y-axis plots the roof-line throughput (assuming no congestion from NoC or L1/L2 read/write).

4. Evaluation

We validated MAESTRO’s runtime results against an open-source hardware RTL source code-based cycle accurate environment called MAERI [15, 1]. On average, the results of MAESTRO presented 94.1% match with the cycle accurate simulation results, as shown in Fig. 15.

4.1. Case study 1: Dataflow Comparison

Fig. 16 presents bandwidth and L1 memory requirements of five dataflows discussed in Table 1. Throughput is measured for a hypothetical 64-PE architecture running in steady state (non-edge regions). Fig. 17 plots the energy consumption across the MAC, L1 and L2 for the same dataflows. We perform this analysis for two CONV layers of VGG16. We emphasize that this is an evaluation of these dataflows’ applicability to this hypothetical architecture, and not meant as a comparison the original systems, which vary widely in number of PEs, buffer sizes, network topology, an so on¹.

We gather useful insights across the dataflows and across layers. Between dataflows, we observe, as expected, that

¹However, for DLA and Shi, a vector read of size 16 and 4 respectively from the L1 is assumed in the energy calculations, instead of multiple expensive scalar reads, as their dataflows are tuned for such an implementation.

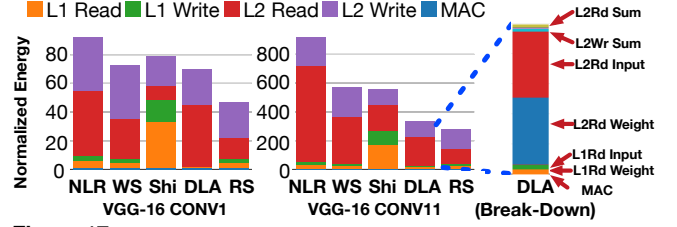


Figure 17: The breakdown of energy consumption of MAC and L1/L2 access for the dataflows from Table 1. The access counts generated by MAESTRO are multiplied by appropriate energy values from Cacti [18] at 28nm for 2KB L1 scratchpad in each PE and 1MB shared L2 buffer. The values are normalized to the MAC energy of NLR.

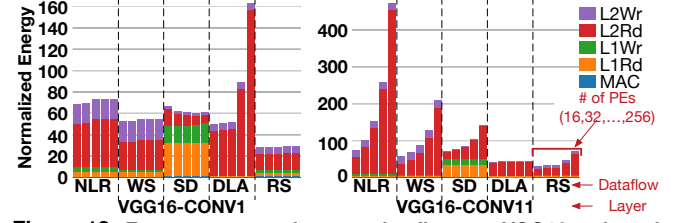


Figure 18: Energy consumption over dataflows on VGG16 early and late layers. We vary the number of PEs in each combination.

NLR has the least L1 memory requirement (as it does not perform temporal reuse at the PE), and therefore has significant L2 energy consumption as presented in Fig. 17. For CONV1, NVDLA dataflow consumes 98% of average amount of energy. However, for CONV11, this trend changes - NVDLA consumes 63% of average amount of energy, which is $2\times$ lower than NLR, WS and Shi, in average. This is because the ratio of input feature map and weight is dramatically different in CONV1(input-dominated) and CONV11(weight-dominated), and NVDLA dataflow is tuned to work efficiently in weight-dominated layers. In detail, CONV1 has just 3 input channels, while CONV11 has 512; NVDLA is tuned for operating on layers with large input channels (as TEMPORAL_MAP (64,64) on variable C of NVDLA dataflow in Table 1 shows), making it inefficient for early layers since it still needs to pay the energy cost of vector reads, but is much more efficient than other dataflows in later layers. For the same reason, NVDLA requires notably high NoC bandwidth in CONV11 (compared to CONV1), since more partial sums get mapped on each PE of NVDLA with CONV11, leading to more L1 to L2 communication for partial sums and outputs. The RS dataflow is observed to be the most energy-efficient due to very few L2 reads demonstrating the best input and weight reuse. Compared to NVDLA, it has much worse roofline throughput in CONV1, but slightly better in CONV11. The Shi dataflow has the highest L1 buffer requirement among all dataflows, as it spatially replicates variable X across 3 PEs and two variables (R and S) are unrolled in each X iteration.

Fig. 18 plots the MAC and buffer access energy with five dataflows on two convolutional layers with the number of PEs 16, 32, 64, 128, and 256. Please note that the number of PEs varies within each dataflow buckets. When we increase the number of PEs, the energy consumption scalability depends

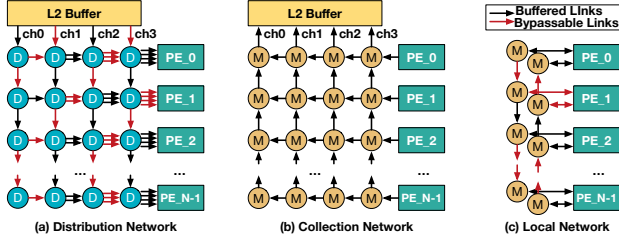


Figure 19: The architecture of FLICR NoC. In the figure, D represents a distribution switch, a single-input-multiple(number of ports are configurable at design time)-output switch, and M represents a merge switch, a two-input two-output switch.

on both of target layer and dataflow, as Fig. 18 presents. Row stationary dataflow scales well in an early layer of VGG16 (CONV1), however, its energy consumption in a late layer of VGG16 (CONV11) increases super-linearly. This sharp increase is because the characteristic of late layer (small input and large number of channels) does not work well with spatially mapped input-columns. Because of the under-utilization of PEs and halo in Y dimension (TEMPORAL_MAP (3,1) Y in Table 1, row-stationary dataflow needs to read the same input data over small tiles, which results in a large number of L2 reads. Because of the good scalability, DLA dataflow performs better with large number of PEs on CONV11. However, DLA dataflow performs worst in CONV1 because of the lack of input/output channels in early layers. Therefore, we need to perform a careful study considering layer dimensions, dataflow characteristics, and also the scalability before we select a dataflow.

4.2. Case study 2: Benefits from Adaptive Dataflows

The analysis from MAESTRO demonstrates quantitatively that no one dataflow is the best across all layers, nor is the same dataflow best from both a throughput and energy-efficiency point of view. Note that automatically finding the best dataflow for a specific CNN layer is beyond the scope of MAESTRO. Its purpose is to serve as a cost model for both manual exploration and future automatic tools. For this work, the point is to conclusively demonstrate the opportunity afforded by being able to use different dataflows for different layers. This requires a NoC interconnect flexible enough to dynamically reconfigure traffic patterns, without being so costly as to overwhelm the area/power benefits [14, 15]. To analyze the hardware cost from NoCs to support adaptive dataflow, we design a NoC named FLICR (Fig. 19) that has full flexibility (multicasting capability and full connectivity) and sufficient bandwidth to support various dataflows based on NoCs proposed in recent works [14, 15]. More details are provided in Table 3. We use the evaluation environment described in Table 2 for hardware cost analysis to support adaptive dataflow using various NoCs.

4.2.1. Performance benefits Fig. 20 presents the benefits of adaptive dataflow in performance and the impact of flexible NoCs on adaptivity. For fixed dataflow, we select DLA and row-stationary (Eyeriss) dataflow with Eyeriss NoC (two-level hierarchical bus). For adaptive dataflow, we select a

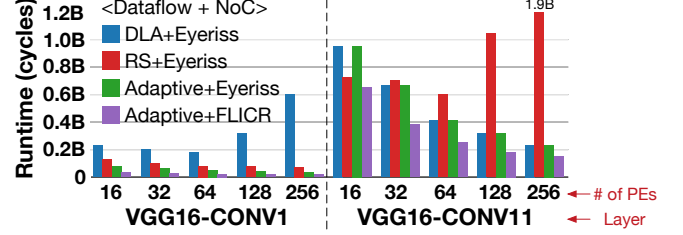


Figure 20: Runtime evaluated using MAESTRO on early (conv1) and late (conv11) layers. We compare the runtime of two fixed dataflow (DLA and RS) on a rigid NoC (Eyeriss) and adaptive dataflow on a rigid NoC (Eyeriss) and FLICR. For adaptive dataflow, WS and DLA dataflows are selected for CONV1 and CONV11, respectively.

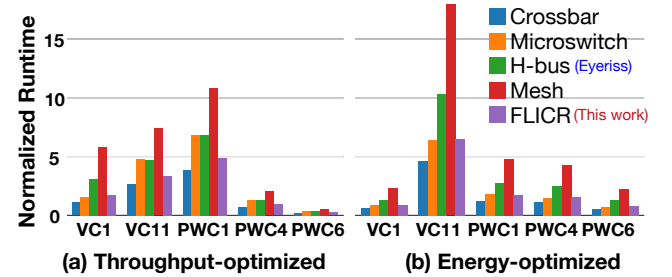


Figure 21: Performance impact of NoCs. (a) and (b) presents runtime from the throughput-optimized dataflow (DLA) energy-optimized dataflow, respectively. We normalized the data to the runtime of crossbar for VGG-16 Conv1 (VC1).

throughput-optimized dataflow for early and late layers of VGG-16, which are weight-stationary and DLA, respectively. We run the selected dataflow on a rigid NoC (Eyeriss) and a flexible NoC (FLICR). To compare the fixed and adaptive dataflow, adaptive dataflow reduced 60.5% of runtime in average compared to two fixed dataflows. We can observe that adaptive dataflow on FLICR provides the lowest runtime over other combinations. Although Eyeriss NoC also provides relatively low runtime with adaptive dataflow compared to fixed dataflows, it requires 70% more runtime compared to FLICR. Also, we can observe that the runtime of row-stationary dataflow does not scale in the late layer. This is because row-stationary dataflow is not optimal in late layers and the bandwidth requirement of row-stationary dataflow increases sharply so NoC congestion introduces enormous delay when we increase the number of PEs.

4.2.2. Runtime impact of NoCs Fig. 21 presents the normalized total run time of the balanced dataflow for two VGGnet layers. Additionally, we evaluate three layers from PWCnet’s Feature Pyramid Extractor [23], a novel contemporary network for optical flow. It exhibits notably different activation-to-weight ratios, and thus acts as a representation of a workload that architects would not have anticipated at design time. Even with the same dataflow, the runtime to run the test layers differed significantly based on the underlying NoC. Crossbar provides the lowest runtime for all the cases because of its high bandwidth. However, it involves significant cost for the throughput as described in Section 4.2.3

Mesh network, which is popular in many-core systems per-

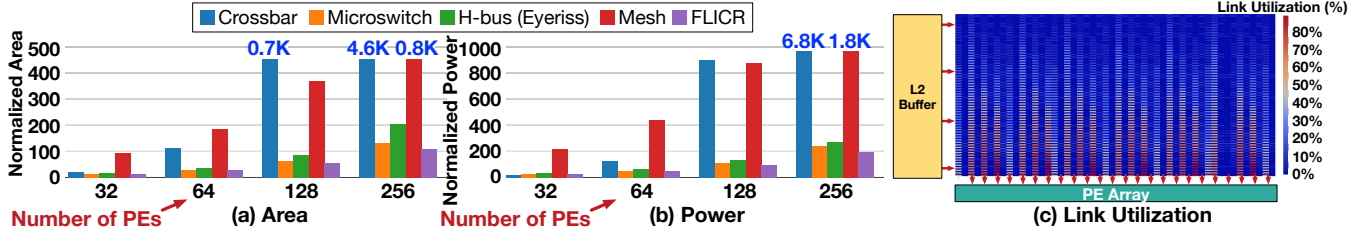


Figure 22: Hardware cost and resource utilization analysis of various NoCs. Area(a) and power(b) of each NoC normalized to those of an Eyeriss [4] PE with different number of PEs. Link utilization heatmap (c) of FLICR's distribution network over 64 PEs.

formed much worse than other options. In contrast, FLICR has shown the second best runtime for most of the test cases. In some cases such as PWC 6 in Fig. 21 (b), the Microswitch NoC outperformed FLICR by 2% because FLICR is internally pipelined while Microswitch NoC pursues single-cycle communication. However, because the pipelined design of FLICR is more suitable to increase clock frequency, we expect such a minor difference can be covered in practice.

4.2.3. Hardware cost of NoCs Fig. 22 (a) and (b) presents post-PnR area and power of each NoCs with different number of PEs. Although crossbar is a good option to provide high throughput, the cost of the throughput is significant. Compared to hierarchical bus, which is popular in recent DNN accelerators [4, 20], a crossbar requires 1.56 times more area and consumes 3.59 times more power. Mesh required the largest area and the second highest power while it performs worst in all the test cases we compare. Hierarchical bus requires moderate area and power with average runtime. Microswitch NoC is a light-weight structure compared to three designs, crossbar, mesh, and hierarchical bus, with low runtime. However, it has less flexibility for different dataflows than FLICR. Furthermore, FLICR reduces the area by 7% with almost the same power consumption.

Fig. 22 (a) and (b) presents a scalability study of NoCs. As presented, FLICR also scales better than other NoC options for both of area and power. With 32 PEs, FLICR consumes 20% more power and 8% more area compared to microswitch NoC. However, with 256 PEs, FLICR requires 56% and 48% less area and 59% and 28% less energy compared to h-bus (Eyeriss NoC) and microswitch NoC. Therefore, FLICR provides not only provides high bandwidth to achieve high accelerator throughput but also requires low hardware cost.

Fig. 22 (c) presents the link utilization of distribution network connected to 64 PEs and four shared buffer channels with Eyeriss-style dataflow (row-stationary). Based on the heatmap and area/power evaluation, we can conclude that FLICR provisions its hardware resources very efficiently for CNN dataflows.

5. Related Works

Dataflow Analysis. Eyeriss [4] categorized dataflows into four classes (weight-, output-, row-stationary and no-local-reuse) based on temporal data reuse pattern, or stationary data class. Flexflow [16] suggested three dataflow categories (featuremap, neuron, and synapse parallelism based on the spatial

Flexibility	Dataflow	Mapping	Buffer access	NoC
Neuflow [8]	Full dataflow processor	Limited by functional units in PE	No local buffer	Flexible but bandwidth limited (bus)
C Brain [22]	Coarse: Three presets	Design time; statically grouped tiles	N/A (not specified)	N/A (not specified)
Flexflow [16]	Coarse: Three presets	Design time; PE row-based mapping	Fixed L1 credit flow; separate FIFOs in L1 and static partitioning in L2	Partially flexible based on 2D bus structure
MAERI [15]	Partially flexible	Fully flexible; run-time virtual neuron construction	Configuration time flexibility	Partially flexible based on augmented reduction tree
FLICR	Fully flexible	Fully flexible	Fully flexible via credit flow	Fully flexible

Table 3: Recent works on flexible dataflow in CNN accelerators

data reuse pattern. MAESTRO provides more fine-grained dataflow description than those two related works, which enables users to describe any dataflow that exploits spatial/temporal data reuse or both at the same time. In compiler side, several works studied the data reuse in the cache of CMPs, the cost and benefits of loop permutations. [12, 17] Although they provided thorough analysis of loop nests in CMP domain, they cannot be directly applied to accelerators because CMPs and accelerators have different architectures (e.g., CMP uses cache memory but accelerators use scratch pad memory).

Flexible Dataflow CNN Accelerators. Table 3 characterizes prior approaches for flexible dataflow support in CNN accelerators with ours.

6. Conclusion

Dataflows play a first-order role in determining the performance, energy consumption, and required hardware resources for accelerators. We present MAESTRO, an analytic model for formally describing and analyzing CNN dataflows using five pragmas that capture various re-use opportunities within CNN accelerators. MAESTRO can be used by architects and hardware designers at design-time to determine the most area/energy/performance efficient design for the target dataflows; it can also be used by compiler writers to determine the most efficient mapping for a CNN layer on the fabric. Extending MAESTRO to model more complex dataflows (such as sparse DNNs, LSTMs) is part of our future work.

References

- [1] Maeri (multiply-accumulate engine with reconfigurable interconnect). <https://github.com/hyoukjun/MAERI>.
- [2] Nvidia deep learning accelerator, 2017. <http://nvidia.org>.
- [3] Tianshi Chen, Zidong Du, Ninghui Sun, Jia Wang, Chengyong Wu, Yunji Chen, and Olivier Temam. Diannao: A small-footprint high-throughput accelerator for ubiquitous machine-learning. In *Proceedings of the International conference on Architectural support for programming languages and operating systems (ASPLOS)*, 2014.
- [4] Yu-Hsin Chen, Joel Emer, and Vivienne Sze. Eyeriss: A spatial architecture for energy-efficient dataflow for convolutional neural networks. In *Proceedings of the International Symposium on Computer Architecture (ISCA)*, 2016.
- [5] Leonardo Dagum and Ramesh Menon. Openmp: an industry standard api for shared-memory programming. *IEEE computational science and engineering (CiSE)*, pages 46–55, 1998.
- [6] Zidong Du, Robert Fasthuber, Tianshi Chen, Paolo Ienne, Ling Li, Tao Luo, Xiaobing Feng, Yunji Chen, and Olivier Temam. Shidiannao: Shifting vision processing closer to the sensor. In *Proceedings of the International Symposium on Computer Architecture (ISCA)*, 2015.
- [7] Clément Farabet, Camille Couprie, Laurent Najman, and Yann LeCun. Learning hierarchical features for scene labeling. *IEEE transactions on pattern analysis and machine intelligence*, 35(8):1915–1929, 2013.
- [8] Clément Farabet, Berin Martini, Benoit Corda, Polina Akselrod, Eugenio Culurciello, and Yann LeCun. Neufow: A runtime reconfigurable dataflow processor for vision. In *Computer Vision and Pattern Recognition Workshops (CVPRW)*, 2011.
- [9] Mingyu Gao, Jing Pu, Xuan Yang, Mark Horowitz, and Christos Kozyrakis. Tetris: Scalable and efficient neural network acceleration with 3d memory. *ACM SIGOPS Operating Systems Review*, 51(2):751–764, 2017.
- [10] Norman P Jouppi, Cliff Young, Nishant Patil, David Patterson, Gaurav Agrawal, Raminder Bajwa, Sarah Bates, Suresh Bhatia, Nan Boden, Al Borchers, et al. In-datacenter performance analysis of a tensor processing unit. In *Computer Architecture (ISCA), 2017 ACM/IEEE 44th Annual International Symposium on*, pages 1–12. IEEE, 2017.
- [11] Andrej Karpathy and Li Fei-Fei. Deep visual-semantic alignments for generating image descriptions. In *Proceedings of the Conference on Computer Vision and Pattern Recognition (CVPR)*, 2015.
- [12] Ken Kennedy and Kathryn S McKinley. Optimizing for parallelism and data locality. In *Proceedings of the 6th international conference on Supercomputing*, pages 323–334. ACM, 1992.
- [13] Hyoukjun Kwon and Tushar Krishna. Opensmart: Single-cycle multi-hop noc generator in bsv and chisel. In *Proceedings of the International Symposium on Performance Analysis of Systems and Software (ISPASS)*, 2017.
- [14] Hyoukjun Kwon, Ananda Samajdar, and Tushar Krishna. Rethinking nocs for spatial neural network accelerators. In *Proceedings of the International Symposium on Networks-on-Chip (NOCS)*, 2017.
- [15] Hyoukjun Kwon, Ananda Samajdar, and Tushar Krishna. Maeri: Enabling flexible dataflow mapping over dnn accelerators via reconfigurable interconnects. In *Proceedings of the International Conference on Architectural Support for Programming Languages and Operating Systems (ASPLOS)*, 2018.
- [16] Wenyan Lu, Guihai Yan, Jiajun Li, Shijun Gong, Yinhe Han, and Xiaowei Li. Flexflow: A flexible dataflow accelerator architecture for convolutional neural networks. In *Proceedings of the International Symposium on High Performance Computer Architecture (HPCA)*, 2017.
- [17] Kathryn S McKinley and Olivier Temam. A quantitative analysis of loop nest locality. In *ACM SIGPLAN Notices*, volume 31, pages 94–104. ACM, 1996.
- [18] N. Muralimanohar et al. Cacti 6.0: A tool to model large caches. *HP laboratories*, pages 22–31, 2009.
- [19] Rishiyur Nikhil. Bluespec system verilog: efficient, correct rtl from high level specifications. In *Proceedings of the International Conference on Formal Methods and Models for System Design (MEMOCODE)*, 2004.
- [20] Angshuman Parashar, Minsoo Rhu, Anurag Mukkara, Antonio Pugliese, Rangharajan Venkatesan, Brucek Khailany, Joel Emer, Stephen W Keckler, and William J Dally. Scnn: An accelerator for compressed-sparse convolutional neural networks. In *Proceedings of the International Symposium on Computer Architecture (ISCA)*, 2017.
- [21] Hardik Sharma, Jongse Park, Divya Mahajan, Emmanuel Amaro, Joon Kyung Kim, Chenkai Shao, Asit Mishra, and Hadi Esmaeilzadeh. From high-level deep neural models to fpgas. In *Proceedings of the International Symposium on Microarchitecture (MICRO)*, 2016.
- [22] Lili Song, Ying Wang, Yinhe Han, Xin Zhao, Bosheng Liu, and Xiaowei Li. C-brain: A deep learning accelerator that tames the diversity of cnns through adaptive data-level parallelization. In *Proceedings of the Design Automation Conference (DAC)*, 2016.
- [23] Deqing Sun, Xiaodong Yang, Ming-Yu Liu, and Jan Kautz. Pwc-net: Cnns for optical flow using pyramid, warping, and cost volume. In *Proceedings of Conference on Computer Vision and Pattern Recognition (CVPR)*, 2018.
- [24] Christian Szegedy, Wei Liu, Yangqing Jia, Pierre Sermanet, Scott Reed, Dragomir Anguelov, Dumitru Erhan, Vincent Vanhoucke, and Andrew Rabinovich. Very deep convolutional networks for large-scale image recognition. In *Proceedings of the International Conference on Learning Representations (ICLR)*, 2015.
- [25] Alexander Toshev and Christian Szegedy. Deeppose: Human pose estimation via deep neural networks. In *Proceedings of the Conference on Computer Vision and Pattern Recognition (CVPR)*, 2014.